

# Quantitative Study of RF field Transmission and Detection Sensitivity Improvements for 3D $^{31}\text{P}$ CSI with Ultrahigh Dielectric Constant Material at 7.0 T

Byeong-Yeul Lee<sup>1</sup>, Sebastian Rupprecht<sup>2</sup>, Xiao-Hong Zhu<sup>1</sup>, Qing X. Yang<sup>3,4</sup>, and Wei Chen<sup>1</sup>

<sup>1</sup>Center for Magnetic Resonance Research, Department of Radiology, University of Minnesota, Minneapolis, MN, United States, <sup>2</sup>Center for Magnetic Resonance Research, Department of Radiology, The Pennsylvania State University College of Medicine, Hershey, PA, United States, <sup>3</sup>Center for NMR Research, Department of Radiology, The Pennsylvania State University College of Medicine, Hershey, PA, United States, <sup>4</sup>Department of Radiology, The Pennsylvania State University College of Medicine, Hershey, PA, United States

**Introduction:** High specific absorption rate (SAR) and inadequate signal-to-noise ratio (SNR) have been major challenges for *in vivo* MRS studies of human brain at high/ultrahigh fields. Previous MR imaging studies have shown a significant benefit for the use of ultra high dielectric constant (uHDC) pad, showing improved  $^1\text{H}$  image SNR with reduced the overall required transmit RF power and SAR at 3T [1]. With consideration of the similar resonance frequency of  $^{31}\text{P}$  on 7.0 T (120.3 MHz) compared to  $^1\text{H}$  on 3.0 T (127.7 MHz), it is of interest and importance to test the effects of uHDC pad on the sensitivity improvement for X-nuclear  $^{31}\text{P}$  MRS application at 7.0T. In the present study, our goals were to: 1) quantitatively examine the improvement of sensitivity for three dimensional (3D)  $^{31}\text{P}$  chemical shift imaging with optimally designed uHDC material at ultrahigh field; and 2) compare the experimental sensitivity results with the enhanced RF transmission and reception fields by the uHDC based on the computer simulation.

## Methods

**Computer Modeling:** For the optimal design of uHDC properties such as a dielectric constant and geometry of pad, transmit efficiency ( $|B_1^+|$ ) and receive sensitivity ( $|B_1^-|$ ) were numerically simulated using a finite difference time domain method (xFDTD) (Remcom, PA, USA), based on the experimental configuration as shown in Fig. 1.

**Design of Coils:** Due to dependence of RF coil performance on the properties of uHDC pad made of lead zirconium titanate (PZT) material (TRS, PA, USA), two multinuclear RF coils were carefully designed for optimal tuning and matching conditions prior to  $^{31}\text{P}$  MRS experiments: a single-loop  $^1\text{H}$  surface coil (d= 8cm) for anatomic imaging and  $B_0$  shimming, and a single-loop  $^{31}\text{P}$  coil (d= 13cm) with reasonable decoupling between the two coils. The  $^{31}\text{P}$  coil was circled around the uHDC pad. A special care was taken for optimal tuning and matching of RF coil under two conditions: one with and another without the use of the uHDC pad.

**$^{31}\text{P}$  MRS:** All  $^{31}\text{P}$  MRS measurements were conducted at 7.0T/90 cm bore human scanner (Siemens). A spherical phantom (d=15cm) filled with 2 liter 20 mM ATP, 40 mM NaCl, and 10 mM  $\text{MgCl}_2$  at pH 7.0 was used for  $^{31}\text{P}$  signal acquisition.  $T_1$  relaxation time of the ATP phantom was 330 ms ( $T_1$  fitting data not shown herein). To investigate the spatial distribution of  $^{31}\text{P}$  SNR and improvement by using the uHDC pad, a 3D chemical shift imaging (CSI) with Fourier Series Window (FSW) technique [2] was applied (TR=2s, FA= 90°, phase encode=  $7 \times 7 \times 5$ , spectral bandwidth= 5 kHz, FOV=  $14 \times 14 \times 10 \text{ cm}^3$ , and hard excitation pulse width= 300 us). The nominal voxel size of 3D CSI was approximate 8 ml, and total acquisition time was 15 min for acquiring each CSI volume. Post-processing included zero-filling the FIDs to 32k data points and 10 Hz line-broadening for enhancing SNR. Spectrum analysis was performed using Lorentzian-curve fitting with AMARES fitting algorithms [3]. In particular, the signals of 18 identified voxels of interest (VOIs) acquired from two CSI slices adjacent to the  $^{31}\text{P}$  coil were analyzed to compare the  $B_1$  simulation results.

**RF Power Calibration:** With double-flip-angle ( $\alpha=30^\circ$ ,  $2\alpha=60^\circ$ )  $B_1$  mapping technique [4], under fully relaxation condition (TR= 2s  $\gg 5 \times T_1$ ), reference RF power for 90° was calibrated for the target voxel located in the center of middle slice (3 cm away from the  $^{31}\text{P}$  coil center). The carrier frequency of the  $^{31}\text{P}$  RF pulse was set to the  $\alpha$ -ATP resonance in which it was used for all spectrum analysis and quantification of SNR.

**Results and Discussion:** Figure 2 shows the simulation modeling results, indicating a clear trend of enhancement of both  $|B_1^+|$  and  $|B_1^-|$  by the optimally designed uHDC material with an ultrahigh dielectric constant ( $\epsilon_{\text{eff}}=1000$ ) for the  $^{31}\text{P}$  operation frequency at 7T. The simulated results of  $B_1$  enhancements were consistent with the experimental results of 3D  $^{31}\text{P}$  CSI (Figs. 3-4). The application of the uHDC pad led to overall SNR enhancement and reduction in the RF power required for achieving the same flip angle. The average RF power (related to  $|B_1^+|$ ) reduction was 45% (53.8 W vs. 97.2 W), and the average SNR (related to  $|B_1^-|$ ) was improved up to 87% with the uHDC pad as illustrated in Fig. 4. More specifically, uHDC pad could affect the  $^{31}\text{P}$  MRS quality by increasing signal and decreasing noise level (Figs. 5-6), resulting in significant improvement of SNR, which is in a good agreement with the prediction based on the simulation results shown in Fig. 2.

**Conclusion:** We demonstrate herein that the use of novel uHDC materials incorporated with RF coil significantly enhances both  $|B_1^+|$  and  $|B_1^-|$ , and increase SNR of  $^{31}\text{P}$  MRS and reducing SAR at 7T. Therefore, *in vivo* x-nuclei will benefit substantially from the uHDC technique, and overcome the challenge of high SAR at high field, aiming for human brain applications. The translation from  $^1\text{H}$  imaging at 3T to  $^{31}\text{P}$  spectroscopy at 7T as demonstrated in this study opens up an avenue for improving other x-nuclear ( $^{17}\text{O}$ ,  $^{23}\text{Na}$  etc.) MRS applications in human at ultrahigh field in which SNR remains a major challenge owing to extremely low metabolites concentration compared to brain tissue water.

**References:** [1] Qing *et al.*, *JMRI* 38:435-440 (2013); [2] Garwood *et al.*, *JMR* 75:244-261 (1987); [3] Vanhamme *et al.*, *JMR*; 129:35-43 (1997); [4] Insko *et al.*, *JMR Ser A* 103: 82-85 (1993). **Acknowledgement:** NIH grants: NS057560, NS070839; S10RR026783 & P41 EB015894.

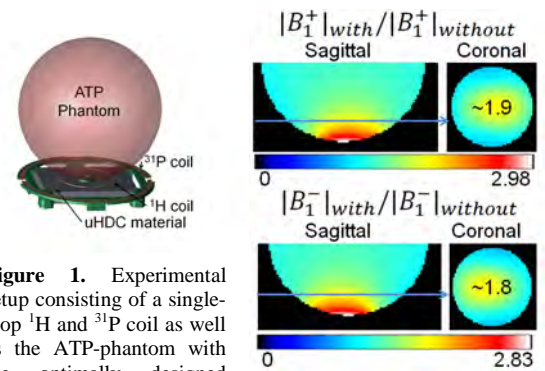


**Figure 1.** Experimental setup consisting of a single-loop  $^1\text{H}$  and  $^{31}\text{P}$  coil as well as the ATP-phantom with the optimally designed uHDC pad (102mm $\times$ 77 mm $\times$ 14 mm).

**Figure 2.** The ratio images of  $^{31}\text{P}$   $B_1$  fields with and without the uHDC pad.  $B_1$  fields were at least 80% higher than that without uHDC in the ROI with 20 mm depth into the phantom.

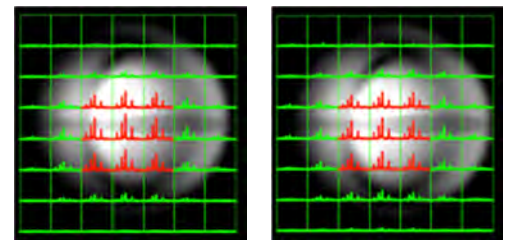


**Figure 3.** 3D chemical shift images of ATP phantom acquired from the middle slice (3 cm away from the  $^{31}\text{P}$  coil) with (left) and without (right) uHDC. The center voxel was used for transmit RF power calibration.

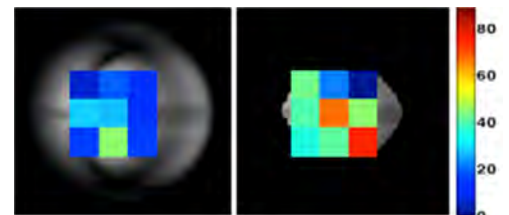


**Figure 4.** SNR maps show global improvement of SNR from 20 up to 87% for target slices: 3cm (left) and 1cm away (right) from the  $^{31}\text{P}$  coil, respectively.

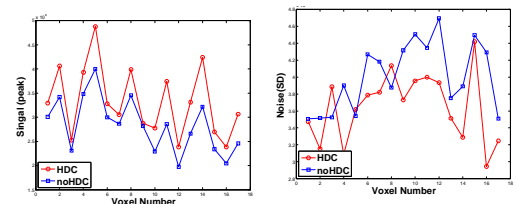


**Figure 5.** Enhancement of signal with HDC.

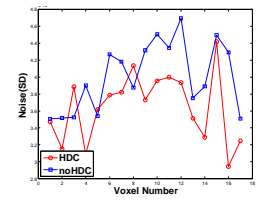


**Figure 6.** Reduction of noise with HDC, leading to a denoising effect.